

SHORT COMMUNICATION

An X-ray method to orientate TiAl single crystals

F. Grégori,^{a*} C. Diot,^b T. Ochin,^b J. Douin^a & P. Veyssi re^a^aLEM, CNRS-ONERA, BP 72, F-92322-Ch tillon-cedex, France^bDirection des Mat riaux, ONERA, BP 72, F-92322-Ch tillon-cedex, France

(Received 2 June 1997; accepted 9 June 1997)

The modest tetragonality of TiAl ($c/a = 1.0184$) makes it difficult to discriminate between the [001] c -axis and the two $\langle 100 \rangle$ a -axes. Based on the utilization of pole figures, the method presented here enables one to orientate single crystals unambiguously by X-ray diffraction. Published by Elsevier Science Limited. All rights reserved.

Keywords: A. titanium aluminides, based on TiAl, B. crystallographic texture.

INTRODUCTION

In the present state of understanding of the plastic properties of TiAl, dedicated experiments in which specific slip systems can be selectively activated are required in order to discriminate between the properties of the various, potential slip systems. Dislocations with three distinct types of Burgers vectors, e.g. $1/2 \langle 110 \rangle$, $\langle 101 \rangle$ and $1/2 \langle 112 \rangle$ (the notation ' $\langle hkl \rangle$ ' refers to any permutation between $\pm h$ and $\pm k$ only, l is specific), may indeed operate and it has been shown that, over a wide range of temperature, each of these can be solicited under appropriate orientations of an uniaxial load.^{1,2} In Ti₄₄Al₅₆ strained below 800°C, deformation may occur via either $\langle 101 \rangle \{111\}$ or $\langle 110 \rangle \{111\}$ slip, the latter system showing a critical resolved shear stress nearly twice as large as that of the former.^{1,2} Despite the fact that the core properties of dislocations with $1/2 \langle 110 \rangle$ Burgers vectors are physically different from those of $\langle 101 \rangle$ superdislocations, in particular with regard to their ability to lock, the temperature dependencies of the flow stress of the $\langle 101 \rangle \{111\}$ and $\langle 110 \rangle \{111\}$ slip systems exhibit similar trends. Typically, the flow stress assumes a rapid decrease with increasing temperature up to room temperature, which is followed by a plateau (better defined, however, for $\langle 101 \rangle \{111\}$ than for $\langle 110 \rangle \{111\}$) that terminates at 600–700°C. Beyond this limit the flow stress increases, to peak at a temperature that depends on the operating slip system. Amongst

many peculiarities, the fact that the Schmid law is violated for $\langle 101 \rangle \{111\}$ slip is noteworthy. Similar to the flow stress anomaly of Ni₃Al-based alloys (L₁₂ structure, for a review see Ref. 3), that of TiAl is accompanied by a number of more or less atypical properties^{1,2} whose origin cannot be elucidated without full control of the operating slip system.

By comparison with the profusion of results on single-crystal L₁₂ alloys, very few straining experiments have been conducted so far on TiAl single crystals.^{1,2,4–9} When the size of the single crystals permitted the selection of a load axis, the orientations of the samples suitable for deformation were determined in two steps. They were pre-oriented by means of the Laue back-reflection X-ray diffraction technique, but because this technique cannot discriminate between diffractions with and without components parallel to the c -axis—which results in an indeterminacy of 90°C (see below)—this first step had to be complemented by an electron diffraction experiment conducted on a thin foil sliced from the pre-oriented single crystal rod. The present contribution is aimed at offering an alternative X-ray method, based on the pole figure method, that enables one to save the above second, lengthy step which could not be avoided until now.

THE LIMITATIONS OF THE LAUE AND EBSD TECHNIQUES

TiAl crystallizes in a tetragonal ordered structure ($tP4$ and $L1_0$ in the Pearson and Strukturbericht

*To whom correspondence should be addressed.

notations, respectively) whose generic representative is AuCu. The cell parameters are close, e.g. $a_{\langle 100 \rangle} = 0.3976 \text{ nm}$ and $c_{[001]} = 0.4049 \text{ nm}$ (determined from the Joint Committee on Powder Diffraction Standards (JCPDS) file no. 5-678, for an estimated composition of $\text{Ti}_{45}\text{Al}_{55}$) and the tetragonality is moderate, $c/a = 1.0184$. Consistently, the angles between the pseudo-cube planes and any octahedral plane are nearly identical ($\phi_{(001)/\{111\}} = 55^\circ 22'$ versus $\phi_{(100)/\{111\}} = 55^\circ 43'$). Since in the Laue method a given diffraction spot represents all $\{h'k'l'\}$ planes such that $h'/h = k'/k = l'/l = p$, where p is an integer, this method is by far too inaccurate to help differentiate between the four-fold $[001]$ and a twofold $\langle 100 \rangle$ zone axis by construction of the stereographic projection.

We have also considered orientating TiAl single crystals by means of electron back-scattered patterns (EBSP). This method is in principle able to discriminate between the $\langle 100 \rangle$ and $\langle 001 \rangle$ axes. The sample is inclined to the beam (Fig. 1) and its normal is determined from the Kikuchi pattern in the direction of the back-scattered electron beam. In practice, the angular range of collection is enough for the Kikuchi patterns to always comprise diffractions with and without components parallel to the c -axis. Identifying the signature of crystal tetragonality is then a matter of being able to discriminate between the real patterns. Differences are exemplified in Fig. 2 where non-equivalent, though comparable simulated patterns are schematically superimposed. Difficulties may arise in practice from the necessity to select the positions of several pairs of Kikuchi lines with the accuracy

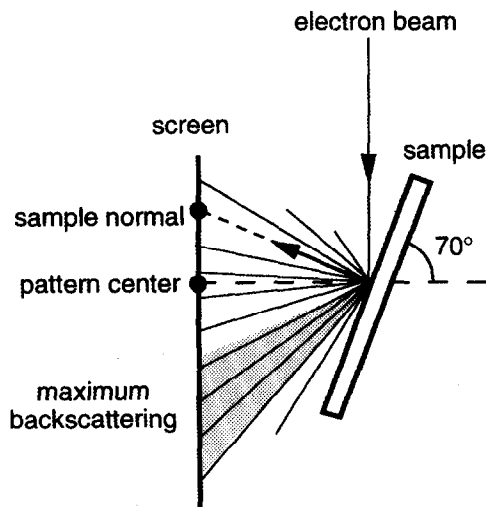


Fig. 1. The EBSD technique: sketch of the orientation of the sample with respect to the incident beam and the location of maximum back-scattered electrons that give rise to the pattern of pseudo Kikuchi lines (see Fig. 2).

appropriate to the slight tetragonality of TiAl. We have tested this method on a TiAl single crystal but we have ended up with a crystal orientation rotated by 90° about a $\langle 100 \rangle$ axis, away from the orientation which we had anticipated from the observed Kikuchi pattern. It appears that the reliability of the EBSP method applied to TiAl depends greatly on the experimental procedure, including the computer-aided part (P. Villechaize, private comm.). In view of the extreme rarity of TiAl single crystals, we have preferred not to pursue this direction.

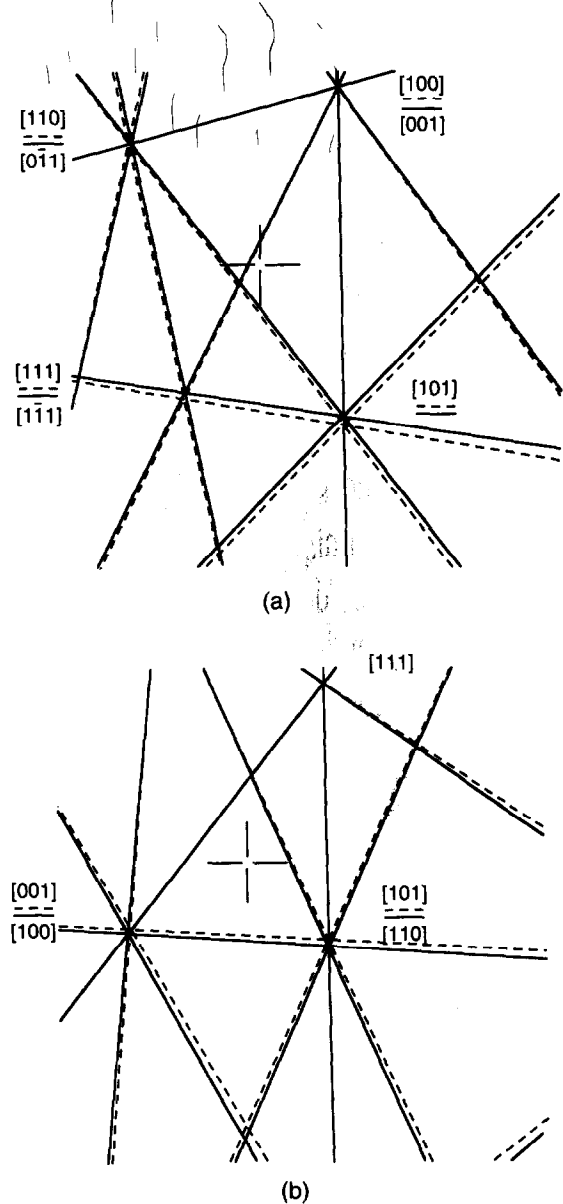


Fig. 2. Comparison between EBSP patterns in TiAl (for the sake of clarity a pair of Kikuchi lines is schematized by one central line; the cross represents the center of an EBSP diagram): (a) superimposition of two patterns corresponding to two non-equivalent pseudo-cubic sample normals while the normal to the detector is kept along the same $[101]$ direction in both cases; (b) superimposition of two patterns corresponding to the same sample normal $([111])$ but the detector normal is set parallel to two non-equivalent $\langle 110 \rangle$ directions.

THE USE OF A POLE FIGURE METHOD TO ORIENTATE TiAl SINGLE CRYSTALS

The preferential crystallographic orientations of textured polycrystals are classically represented by construction of their pole figure. This method takes advantage of the property that each (hkl) pole corresponds to a well-defined Bragg angle $2\theta_{(hkl)}$ and, in distinction to the Laue technique, it makes use of monochromatic X-ray radiation. The sample is tilted by steps of 5° of the Euler angular co-ordinates (φ, ψ) over a solid angle of nearly 2π . When the counter, set at $2\theta_{hkl}$ with respect to the source, detects a signal, the corresponding co-ordinates (φ, ψ) are plotted on a stereographic projection. The iso-intensity lines thus obtained constitute the pole figure of the textured sample.

In TiAl the Bragg angles corresponding to the poles (002) and (200) are sufficiently distinct to be differentiated angularly ($2\theta_{(002)} = 52.439^\circ$ versus $2\theta_{(200)} = 53.478^\circ$ from the JCPDS file; the instrumental accuracy on the measurements of 2θ is of 0.01°). It is thus possible to locate and to identify these by scanning the sample over the near- 2π solid angle for each of the two values of $2\theta_{(hkl)}$ (the experimental device consists of a Euler circle fitted to a $\theta-2\theta$ Seifert K-IV goniometer; the slit in front of the counter is about 0.3 mm wide). We have performed this type of scanning on single crystals just as one would proceed with a textured polycrystal. The difference is that each pole of the single crystal pole figure corresponds of course to one single set of co-ordinates (φ, ψ) of the stereographic representation. Hence, a pole figure of a single crystal constructed with the three pseudo-cubic axes will consist of three well-defined spots, the (002) pole being unambiguously discriminated.

In practice, φ is varied between 0° and 360° and ψ from 0° to 85° , in steps of 5° ; an integration time of 1 s per angular step is ample for the search of the (002) and (200) reflections. The application of this method is exemplified in Figs 3–5 which represent the stereographic projection of the single crystal for three discrete and close values of $2\theta_{(hkl)}$, namely 54° , 54.5° and 55° . It should be noted that, in fact, the experimental values of $2\theta_{(hkl)}$ cannot be known directly with sufficient precision from the knowledge of the crystal composition, which itself may in addition not be fully homogeneous. In order to avoid confusion, we have performed for our specific crystal composition a systematic search of the true values of $2\theta_{(200)}$ and $2\theta_{(002)}$. This has been done, again by means of the pole figure method, within a limited range of 2θ values. We have found

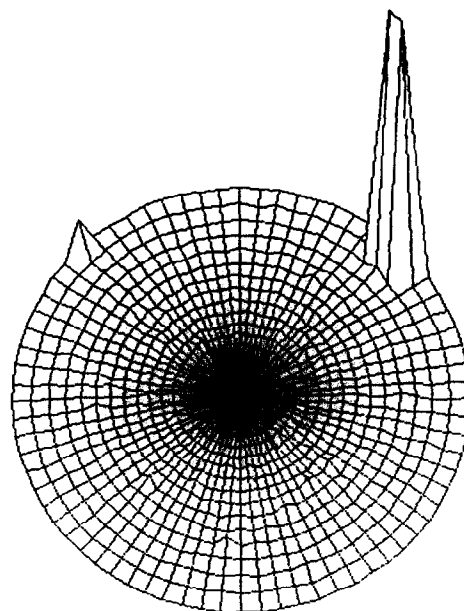


Fig. 3. Pole figure obtained upon setting 2θ at 54° . Note the prominence of the (002) peak for $\varphi = 155^\circ$ and $\psi = 80^\circ$. The intensity of the peak, I_{\max} is about $850 \text{ counts s}^{-1}$ (the intensity scale is different in from those of Figs 4 and 5).

that the true values of $2\theta_{(200)}$ and $2\theta_{(002)}$ are in fact located between 54° and 55° , that is, within about the same angular range of 1° as indicated by the JCPDS file, though shifted to higher angles by about 1.5° .

In Fig. 3 ($2\theta = 54^\circ$), the position of the (002) pole is clear and unique and no pole other than (002) emerges significantly. For $2\theta = 54.5^\circ$, located past (002) though not quite appropriate for {200} reflections, two peaks are clearly visible (Fig. 4), that of (002) which shows a higher intensity and lesser spread than in Fig. 3, and that corresponding to (200), located near the center of the stereographic projection (somewhat hidden by the mode of display). Consistently, the third pole, (020), must be located in the vicinity of the great outer circle off the solid angle scanned so that only its tail is detected (visible in Figs 3–5). Figure 5 shows the pole figure recorded under $2\theta = 55^\circ$ which exhibits an intense (200) peak, while the (020) peak is not as intense (note that it is for this angle that the recorded peak intensity is the highest). From the relative intensities of the (002) peaks of Figs 3–5, we may conclude that for the composition under consideration $2\theta_{(002)}$ is actually located between 54° and 54.5° (we have checked that (002) has almost vanished for $2\theta = 54.8^\circ$). Both the (200) and (020) poles are simultaneously evidenced for $2\theta = 55^\circ$ (Fig. 5) and one can check that the three poles are at 90° from each other in the stereographic projection.

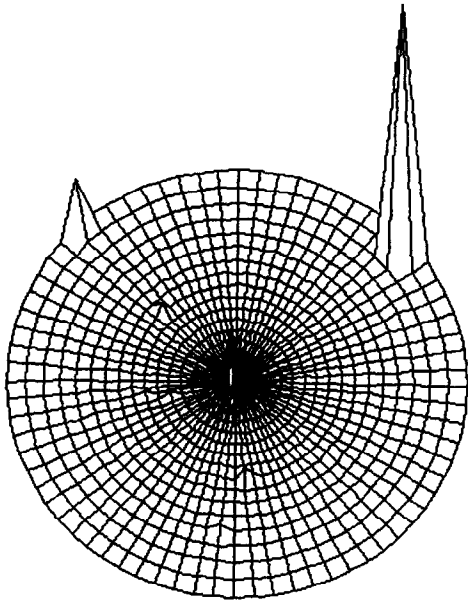


Fig. 4. Pole figure for $2\theta = 54.5^\circ$. The (002) peak is still present, while the (200) peak emerges for $\varphi = 60^\circ$ and $\psi = 85^\circ$ (a maximum intensity of $I_{\max} \approx 1450$ counts s^{-1} in both cases). The (020) peaks are hardly visible at $\varphi = 300^\circ$ and $\psi = 10^\circ$.

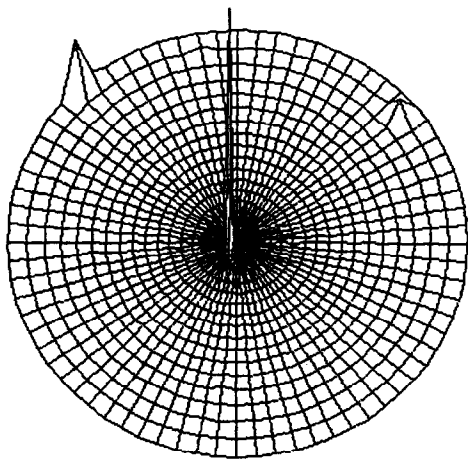


Fig. 5. Pole figure for $2\theta = 55^\circ$. The (002) pole is disappeared. The (200) peak shows a maximum intensity of 3000 counts. Again the (020) peak is faintly visible.

As a complementary test we have produced the stereographic projection of the same crystal for the (003) reflection ($2\theta_{(003)} = 83.75^\circ$) and found its position at the same (φ , ψ) co-ordinates as for

(002). In view of the weakness of this reflection, the integration time had to be a hundred times longer.

Finally, we should mention that, in practice, the fully oriented single crystal is subsequently fixed to a holder compatible with the spark-machining device. This requires that, during the transfer, one roughly keeps track of the orientations of the pseudo-cubic axes and that an additional Laue pattern be taken to ensure that crystallographic orientation of the sample with respect to the holder tilt axes is determined reasonably accurately.

ACKNOWLEDGEMENTS

The assistance of Thierry Baudin (Laboratoire de Métallurgie Structurale—Orsay) during the EBSD experiments is gratefully acknowledged. The simulations of EBSD patterns were kindly provided by Dr Patrick Villechaise (Laboratoire de Mécanique et de Physique des Matériaux—Poitiers). The latter together with Dr P. H. Jouneau are gratefully thanked for helpful discussions.

REFERENCES

1. Kawabata, T., Kanai, T. and Izumi, O., *Acta metall.*, 1985, **33**, 1355.
2. Inui, H., Matsumuro, M., Wu, D.-H. and Yamaguchi, M., *Phil. Mag. A*, 1997, **75**, 395.
3. Veyssi re, P. and Saada, G., in *Dislocations in Solids*, Vol. 10, ed. F. R. N. Nabarro and H. S. Duesbery. Elsevier Science, Amsterdam, 1996, p. 255.
4. Kawabata, T., Abumiya, T., Kanai, T. and Izumi, O., *Acta metall. mater.*, 1990, **38**, 1381.
5. Li, Z. X. and Whang, S. H., *Mater. Sci. Engng.*, 1992, **A152**, 182.
6. Wang, Z.-M., Li, Z. X. and Whang, S. H., *Mater. Sci. Engng.*, 1995, **A192-193**, 211.
7. Stucke, M. A., Dimiduk, D. M. and Hazzledine, P. H., in *High Temperature Ordered Intermetallics V*. MRS Symp. Proc. 288, 1993, p. 471.
8. Stucke, M. A., Vasudevan, V. K. and Dimiduk, D. M., *Mater. Sci. Engng.*, 1995, **A192-193**, 111.
9. Bird, N., Taylor, G. and Sun, Y. Q., in *High Temperature Ordered Intermetallics XVI*. MRS Symp. Proc. 364, 1995, p. 635.